Journal of Coordination Chemistry

ISSN: 0095-8972 (Print) 1029-0389 (Online) Journal homepage: http://www.tandfonline.com/loi/gcoo20

# A density functional theory study of the $Cu^{+}\cdot(CO)_n$ (n = 1–3) complexes

Ismail I. Fasfous, Jamal N. Dawoud, Abdulwahab K. Sallabi & Taghreed S. Hassouneh

**To cite this article:** Ismail I. Fasfous, Jamal N. Dawoud, Abdulwahab K. Sallabi & Taghreed S. Hassouneh (2015) A density functional theory study of the $Cu^{+}\cdot(CO)_n$ (n = 1–3) complexes, Journal of Coordination Chemistry, 68:9, 1528-1543, DOI: 10.1080/00958972.2015.1021343

**To link to this article:** http://dx.doi.org/10.1080/00958972.2015.1021343

Accepted author version posted online: 23 Feb 2015.
Published online: 20 Mar 2015.

*Journal of Coordination Chemistry*, 2015
Vol. 68, No. 9, 1528–1543, http://dx.doi.org/10.1080/00958972.2015.1021343



# A density functional theory study of the $Cu^{+}\cdot(CO)_n$ ($n$ = 1–3) complexes

ISMAIL I. FASFOUS†, JAMAL N. DAWOUD*†, ABDULWAHAB K. SALLABI‡ and TAGHREED S. HASSOUNEH†

†Department of Chemistry, Hashemite University, Zarqa, Jordan
‡Department of Physics, Misurata University, Misurata, Libya

(*Received 24 June 2014; accepted 29 January 2015*)

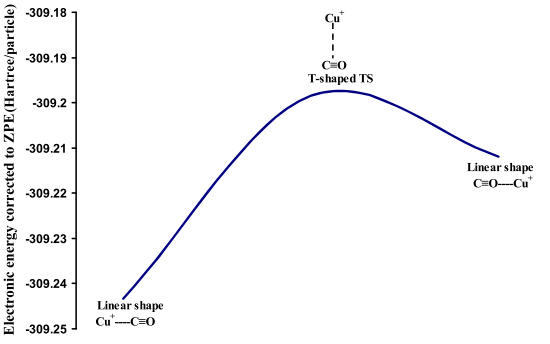


Density functional theory calculations, with an effective core potential for the copper ion, and large polarized basis set functions have been used to construct the potential energy surface of the $Cu^{+}\cdot(CO)_n$ ($n$ = 1–3) complexes. A linear configuration is obtained for the global minimum of the $Cu^{+}\cdot CO$ and $Cu^{+}\cdot(CO)_2$ complexes with a bond dissociation energy (BDE) of 35.9 and 40.0 kcal mol$^{-1}$, respectively. For the $Cu^{+}\cdot(CO)_3$ complex, a trigonal planar geometry is obtained for the global minimum with a BDE of 16.5 kcal mol$^{-1}$. C-coordinated copper ion complexes exhibit stronger binding energy than O-coordinated complexes as a result of $C_{lp} \rightarrow 4s$ $\sigma$-donation. The computed sequential BDEs of $Cu^{+}\cdot(CO)_n$ ($n$ = 1–4) complexes agree well with experimental findings, in which the electrostatic energy and $\sigma$-donation play an important role in the observed trend.

*Keywords*: Density functional theory; Carbon oxides; Copper; $\sigma$-Donation; Potential energy surface

## Introduction

Metal carbonyl chemistry is often used as starting materials in organometallic synthesis and their chemistry is useful to characterize extra-framework metal cations in zeolites. Special attention was also given to activation of the C–O and N–O bonds in some important

*Corresponding author. Email: jamaldawoud@hu.edu.jo
This article was originally published with errors. This version has been corrected. Please see Erratum (http://dx.doi.org/10.1080/00958972.2015.1035522) and Corrigendum (http://dx.doi.org/10.1080/00958972.2015.1041283).

pollutants (NO, CO, $NO_2$, and $CO_2$) [1–3]. Therefore, the removal of these contaminant gasses was extensively studied theoretically and experimentally. These studies have examined the catalytic CO oxidation using different methods [4] and interaction process to understand the bonding mode of the $Cu^+{\cdot}CO$ complex in its electronic ground state [5–7], since these complexes may indicate the presence of $\sigma$- or $\pi$-back donation. In addition, the bond dissociation energies (BDEs) of $Cu^+{\cdot}(CO)_n$ ($n$ = 1–4) complexes were determined by guided ion beam mass spectrometry [8]. These experimental findings show that sequential BDEs of these complexes followed a specific trend.

Numerous theoretical studies have been reported on the interaction between $Cu^+$ and CO molecule so as to determine the nature of the active site of Cu-zeolite and examine the structures where the complex only exists in its minimum state using different kinds of *ab initio* methods [6, 9, 10]. Furthermore, the bonding mode among the $Cu^+$ and many CO molecules was also investigated to determine the geometries and their BDEs [11–13]. However, the primary issues to be considered here are the discrepancies between the experimental findings of the BDE trend [8] and the results obtained by the B3LYP and BP86 calculation methods for the $Cu^+{\cdot}(CO)_n$ ($n$ = 1–4) complexes [11, 13]. In particular, these calculations showed that the mono-ligated complex has the largest BDE value, which disagrees with the experimental findings (the di-ligated complex exhibits the largest BDE value). Furthermore, the CCSD(T) calculations of the BDEs of the $Cu^+{\cdot}(CO)_n$ ($n$ = 1–4) complexes were lower than those of the reported experimental data by 5–6 kcal $mol^{-1}$ for the mono- and di-ligated complexes [12]. Despite these efforts, the specific BDE trend of the $Cu^+{\cdot}(CO)_n$ ($n$ = 1–4) complexes has not been explained in detail and hence is revisited in this work.

In this article, we attempt to construct the structures and potential energy surfaces of the $Cu^+{\cdot}(CO)_n$ complexes, $n$ = 1–3, using different levels of density functional theory (DFT), where the structures, and binding energies (BEs) are determined for the global, local, and transition states. Only the global minima structures of the C-coordinated copper ion complexes, $Cu^+{\cdot}(CO)_n$, are reported experimentally and theoretically in the literature while other structures mentioned in this article are new and studied theoretically for the first time. The BDEs of $Cu^+{\cdot}(CO)_n$ complexes, $n$ = 1–4, are also examined. Our results are then compared with the available experimental and theoretical data reported in the literature.

## Computational details

All theoretical calculations are carried out by the Gaussian 03 program suite [14]. The geometries and harmonic vibration frequencies of the $Cu^+{\cdot}(CO)_n$ complexes ($n$ = 1–3) are optimized at various levels of hybrid DFT theory. In particular; B3LYP, B3P86, and B3PW91 calculations of these complexes are performed using different types of polarization and diffuse basis sets such as 6-31+G(d) and 6-311+G(df). These basis sets have only applied for the CO molecule. There are a limited number of basis sets that are suitable to be applied for $Cu^+$ ion. In this work, the effective core Los Alamos (LANL2DZ and polarized LANL2TZ+, available from EMSL basis set exchange, https://bse.pnl.gov/bse/portal, [15, 16]) pseudopotentials (ECPs) have been used for $Cu^+$. Therefore, the computational protocols are denoted as for example, B3LYP/6-31+G(d)(CO)/LANL2TZ+($Cu^+$). These DFT methods have provided reasonably good geometries, energies values, and vibration frequencies for studying transition metal ion complexes, such as $Cu^+$ [17, 18] and $Zn^{2+}$ [19]

with different kinds of molecules, second row transition dimers [20], Au, and Pt clusters anions [21] and organic reaction in which these metals were involved [22]. Bühl *et al*. showed that hybrid DFT methods such as B3P86, B3PW91, and PBE0 are recommended for transition metal–ligand bond distances over the non-hybrid DFT methods such as LSDA and VSXC [23]. However, Truhlar *et al*. have shown that use of pure and hybrid DFT methods depends on the goal of the calculations [24], in particular B3LYP failed to describe the properties of bulk transition metals such as lattice constant, bulk moduli, and cohesive energy, whereas it works best for predicting the adsorption energy of CO on the surface of these metals. Additionally, hybrid DFT methods yielded more reasonable geometrical parameters and BEs for copper cation complexes, $[Cu{\cdot}CO]^{+}$, than for neutral and anionic copper complexes with CO species, $[Cu{\cdot}CO]^{0,-}$ [13]. Thus, the hybrid DFT methods applied in this work are suitable to study the complexes of copper ion with CO molecules and agreed well with the reported literature data.

Together the intrinsic reaction coordinate (IRC) [25, 26] and the vibration frequency tests are performed to determine which minimum does the saddle point and calculate the zero-point energy for each stationary point at $T = 298$ K. The BE is determined from the difference between the total energy of the complex minus the total energies of the uncomplexed cation and diatomic molecule as applied elsewhere [27]. The obtained energy is then corrected for basis set superposition error (BSSE) using the full counterpoise method [28, 29].

To have insight into the electronic structures and bonding properties of the investigated complexes, the electronic parameters and molecular orbital (MO) diagrams of these complexes, at different structures, are carried out according to the natural bond orbital (NBO) analysis [30]. The amount of electronic transfer occurring within the complex is determined by calculating the second-order energy of interaction given by

$$E^{(2)} = \frac{-2 \cdot F_{ij}}{\Delta E_{ij}} \tag{1}$$

where $\Delta E_{ij} = E_i - E_j$ is the energy difference between the interacting MOs $i$ and $j$; $F_{ij}$ is the Fock matrix element for the interaction between orbitals $i$ and $j$. In addition, $F_{ij}$ represents the occupancy of acceptor orbitals in these adducts as applied elsewhere [31–33]. $\sigma$-donation involves electronic transfer from nonbonding electron lone pairs of carbon of CO toward the 4s orbital of the naked $Cu^{+}$ ion, $C_{lp} \rightarrow 4s$, whereas the opposite trend is attributed to the $\pi$-back donation ($3d \rightarrow \pi^{*}_{2p}$). Note here that electronic transfer, $C_{lp} \rightarrow 4s$, is the prevalent $\sigma$-donation as applied for metal carbonyl complexes [7, 34]. Therefore, special attention is paid to this electronic channel to estimate the amount of the electronic transfer within the complex. These calculations are performed using the B3P86/6-311+G (df)/LANL2DZ method.

The sequential BDEs of the $Cu^{+}{\cdot}(CO)_n$ complex are calculated at different orientations for the global and local states according to the following equation,

$$Cu^{+} \cdot (CO)_n \longrightarrow Cu^{+} \cdot (CO)_{n-1} + CO \quad (n : 1 - 4)$$

To reproduce the experimental trend of the BDEs, the atomic charge distributions of the $Cu^{+}{\cdot}(CO)_n$ complex at different configurations are calculated, according to the NBO analysis. For simplicity, the charge distribution spread over an orbital centered at a particular atom is treated as a point charge at the location of the atom as applied elsewhere [35]. Using these point charges, the electrostatic contribution, $E_{elec.}$, to the BDE of the $Cu^{+}{\cdot}(CO)_n$

complex is calculated as a pairwise sum of point charges located on each atomic site of CO and $Cu^+$ ion using the following formula,

$$E_{\text{elec.}} = -\frac{q_{\text{Cu}}}{4\pi\varepsilon_{\text{o}} n}\sum_{n=1}^{4}\left(\frac{q_{\text{C}}}{r_{\text{Cu-C}}}+\frac{q_{\text{O}}}{r_{\text{Cu-O}}}\right)_{\text{n}} \quad n = 1-4 \tag{2}$$

where $n$ represents the number of CO molecules in the complex; $q_{\text{Cu}}$, $q_{\text{C}}$ and $q_{\text{O}}$ are the point charges located on $Cu^+$, C, and O atoms, respectively, $r_{\text{Cu–C/O}}$ is the distance between the $Cu^+$ ion and C/O in the complex; and $\varepsilon_{\text{o}}$ is the permittivity of the vacuum.

## Results and discussion

### *The $Cu^+$·CO complex*

The IRC of the $Cu^+$·CO complex ($^1\Sigma^+$) performed at the B3LYP level of theory showed the existence of one transition (T-shaped) and two minima (linear structure) states as shown in figure 1. The optimized geometrical parameters of the $Cu^+$·CO complex at different orientations are given in table 1. The global minimum is formed when the $Cu^+$ is directly bonded with the carbon site at a distance of $r_{(\text{Cu–C})} = 1.892$ Å and $r_{(\text{C–O})} = 1.115$ Å [calculated on the basis of the B3LYP/LANL2TZ+/6-31+G(d)], which agreed well with other theoretical calculations that yielded similar geometrical parameters (see table 1) [6, 9, 36]. Our best value of the CO bond length agreed well with the bond length of free CO [37]. The second local minimum is obtained when the $Cu^+$ is directly bonded to the oxygen site at a distance of $r_{(\text{Cu–O})} = 2.003$ Å and $r_{(\text{C–O})} = 1.141$ Å, which is longer than the bond length of free CO molecule. The T-shaped structure of the complex is found to be a transition state, where its structural parameters are $r_{(\text{Cu–C})} = 2.331$ Å and $r_{(\text{C–O})} = 1.147$ Å and $\angle_{(\text{Cu–C1–O2})} = 69.8°$. The harmonic frequency calculations of the $Cu^+$·CO complex (result not shown) showed that our best values for the two minima exist at 2320 $cm^{-1}$ ($Cu^+$–CO) and 2127 $cm^{-1}$ ($Cu^+$–OC). These results, calculated on the basis of the B3LYP/LANL2TZ/6-311+G(df)

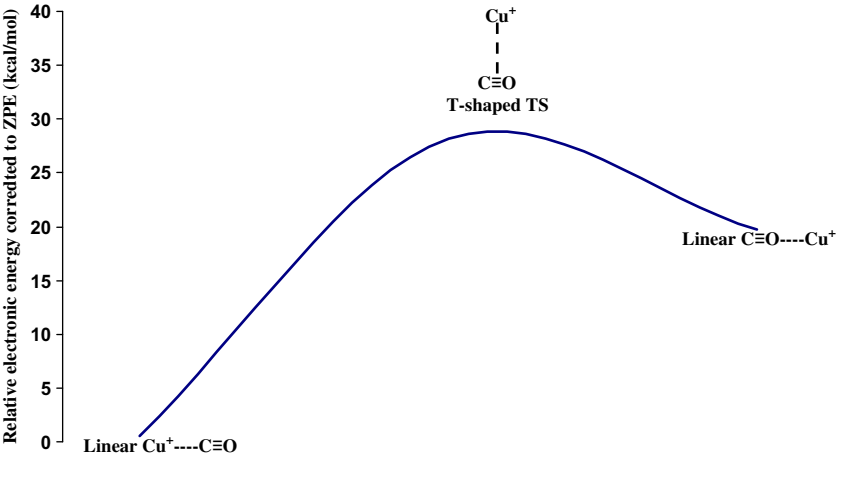


Figure 1. The IRC diagram of the $Cu^+$·CO complex calculated at the B3LYP/LANL2DZ/6-311+G(df) level of theory.

Table 1. Geometrical parameters of the $Cu^+$·CO complex[a] at different configurations.

| Geometry | Method | Basis set | $r_{(C-O)}$ | $r_{(Cu-C)}$ | $r_{(Cu-O)}$ | $\theta(°)$[b] | $\theta(°)$[c] |
|---|---|---|---|---|---|---|---|
| Linear $Cu^+$·CO | B3LYP | LANL2DZ/6-31+G(d) | 1.125 | 1.933 | – | 180.0 | – |
| | | LANL2DZ/6-311+G(df) | 1.115 | 1.924 | – | 180.0 | – |
| | | LANL2TZ+/6-31+G(d) | 1.125 | 1.902 | – | 180.0 | |
| | | LANL2TZ+/6-311+G(df) | 1.115 | 1.892 | – | 180.0 | – |
| Free CO | | 6-311+G(df) | 1.126 | – | – | – | – |
| | B3PW91 | LANL2DZ/6-31+G(d) | 1.124 | 1.921 | – | 180.0 | – |
| | | LANL2DZ/6-311+G(df) | 1.115 | 1.908 | – | 180.0 | – |
| | | LANL2TZ+/6-31+G(d) | 1.125 | 1.890 | – | 180.0 | |
| | | LANL2TZ+/6-311+G(df) | 1.115 | 1.876 | – | 180.0 | – |
| Free CO | | 6-311+G(df) | 1.126 | – | – | – | – |
| | B3P86 | LANL2DZ/6-31+G(d) | 1.124 | 1.912 | – | 180.0 | – |
| | | LANL2DZ/6-311+G(df) | 1.114 | 1.899 | – | 180.0 | – |
| | | LANL2TZ+/6-31+G(d) | 1.124 | 1.882 | – | 180.0 | |
| | | LANL2TZ+/6-311+G(df) | 1.115 | 1.869 | – | 180.0 | – |
| Free CO | | 6-311+G(df) | 1.125 | – | – | – | – |
| Linear $Cu^+$·CO | MCPF[d] | ECP/primitive Gaussian sets (d,p) | 1.127 | 1.940 | – | 180.0 | – |
| Linear $Cu^+$·CO | BP86[e] | LSDA | 1.121 | 1.807 | – | 180.0 | – |
| Linear $Cu^+$·CO | BLYP[f] | TZP | 1.137 | 1.769 | – | 175.0 | |
| Linear $Cu^+$·CO | B3LYP[g] | cc-pVTZ/TZV2P | 1.115 | 1.897 | – | 180.0 | – |
| Linear $Cu^+$·OC | B3LYP | LANL2DZ/6-31+G(d) | 1.151 | – | 2.028 | – | 180.0 |
| | | LANL2DZ/6-311+G(df) | 1.140 | – | 2.023 | – | 180.0 |
| | | LANL2TZ+/6-31+G(d) | 1.151 | – | 2.009 | – | 180.0 |
| | | LANL2TZ+/6-311+G(df) | 1.141 | – | 2.003 | – | 180.0 |
| | B3PW91 | LANL2DZ/6-31+G(d) | 1.150 | – | 2.033 | – | 180.0 |
| | | LANL2DZ/6-311+G(df) | 1.141 | – | 2.026 | – | 180.0 |
| | | LANL2TZ+/6-31+G(d) | 1.151 | – | 2.013 | – | 180.0 |
| | | LANL2DZ+/6-311+G(df) | 1.140 | – | 2.005 | – | 180.0 |
| | B3P86 | LANL2DZ/6-31+G(d) | 1.150 | – | 2.014 | – | 180.0 |
| | | LANL2DZ/6-311+G(df) | 1.139 | – | 2.009 | – | 180.0 |
| | | LANL2TZ+/6-31+G(d) | 1.150 | | 1.994 | – | 180.0 |
| | | LANL2TZ+/6-311+G(df) | 1.140 | – | 1.987 | – | 180.0 |
| T-shaped TS | B3LYP | LANL2DZ/6-31+G(d) | 1.146 | 2.363 | – | 70.5 | – |
| | | LANL2DZ/6-311+G(df) | 1.135 | 2.406 | – | 68.5 | – |
| | | LANL2TZ+/6-31+G(d) | 1.147 | 2.331 | – | 69.8 | – |
| | | LANL2TZ+/6-311+G(df) | 1.136 | 2.384 | – | 68.1 | – |
| | B3PW91 | LANL2DZ/6-31+G(d) | 1.146 | 2.371 | – | 68.8 | – |
| | | LANL2DZ/6-311+G(df) | 1.136 | 2.421 | – | 66.6 | – |
| | | LANL2TZ+/6-31+G(d) | 1.148 | 2.343 | – | 67.7 | – |
| | | LANL2DZ+/6-311+G(df) | 1.137 | 2.399 | – | 66.0 | – |
| | B3P86 | LANL2DZ/6-31+G(d) | 1.146 | 2.338 | – | 68.8 | – |
| | | LANL2DZ/6-311+G(df) | 1.135 | 2.388 | – | 66.5 | – |
| | | LANL2TZ+/6-31+G(d) | 1.148 | 2.315 | – | 67.7 | – |
| | | LANL2TZ+/6-311+G(df) | 1.137 | 2.371 | – | 65.8 | – |

[a]All bond lengths are in (Å) and bond angles are in degrees.
[b]∠Cu–C1–O2 bond angle.
[c]∠Cu–O2–C1 bond angle.
[d]Taken from Ref. [36].
[e]Taken from Ref. [9].
[f]Taken from Ref. [6].
[g]Taken from Ref. [13].

method, agreed well with other DFT calculations (2222 $cm^{-1}$ [5], 2238 $cm^{-1}$ [10], and 2263 $cm^{-1}$ [38]) and with an experimental determination value of 2157 $cm^{-1}$ [5, 39].

The NBO electronic population analysis of the corresponding orbital between the metal ion and CO is calculated and compared with those of $Cu^+$ ion and CO molecule before complexation as presented in table 2. In all configurations, the outer shell electron density of $Cu^+$ is redistributed, where a small electronic charge transfers from 3d orbitals

Table 2. NBO analysis of natural charges, 3d, and 4s populations of $Cu^+$ and total population of the valence shell of each atomic site in CO at different structures on the basis of the B3P86/LANL2DZ/6-311+G(df) method.

| | $Cu^+$ | CO | $Cu^+$·CO (minim I) | $Cu^+$·CO (T-shaped TS) | $Cu^+$·OC (minim II) |
|---|---|---|---|---|---|
| $q_{Cu}$ | +1.000 | – | +0.916 | +0.973 | +0.994 |
| 3d | 10.000 | – | 9.884 | 9.968 | 9.962 |
| 4s | 0.000 | – | 0.201 | 0.055 | 0.041 |
| Symmetry | – | – | $C_{\infty\ v}$ | – | $C_{\infty\ v}$ |
| $\sigma$-donation($C/O_{lp} \rightarrow 4s$) | – | – | 0.085 | 0.023 | – |
| $\pi$-back donation($3d \rightarrow \pi^*_{2p}$) | – | – | 0.041 | 0.015 | 0.018 |
| $(2s,2p_{x,y,z})$ C | – | 3.470 | 3.577 (▲0.107) | 3.408 (▼0.062) | 3.258 (▼0.212) |
| $(2s,2p_{x,y,z})$ O | – | 6.462 | 6.260 (▼0.202) | 6.491 (▲0.029) | 6.673 (▲0.211) |

Note: ▲: amount of increase relative to the atomic site in free CO, ▼: amount of decrease relative to the atomic site in free CO.



[$3d^1 \rightarrow 3d^{9.884}$ (linear $Cu^+$·CO), $3d^{9.962}$ (linear $Cu^+$·OC), and $3d^{9.968}$ (T-shaped TS)] toward the 4s orbital as a result of interaction with CO. In addition, the population at the 4s orbital increases when the $Cu^+$ ion bonded to carbon of CO, indicating that a sizable charge transfer from the CO lone pair to the metal ion has taken place. The depletion of the 3d population and the increase of the 4s population predict some 3d–4s mixing (hybridization). This reduces the metal–CO repulsion and enhances the bonding especially in the global minimum structure. For CO, the $\pi$ electrons are highly polarized in which the electrons migrate toward the C/O atomic site that is nearest to $Cu^+$ ion as a result of attraction between them (see table 2). For the T-shaped structure, the polarization of $\pi$ electrons is insignificant since the interaction between the $Cu^+$ ion and CO moiety is very weak. Furthermore, the atomic charges of the $Cu^+$ in three orientations of the $Cu^+$·CO complex indicate that the complex in its global minimum has a larger electronic charge transfer ($\sigma$-donation) between its components than that of the local minimum and hence exhibits a larger BE. For the T-shaped structure, TS, the variation in the Cu atomic charge is insignificant. Note here that $\pi$-back donation, $3d \rightarrow \pi^*_{2p}$, is relatively weak in all $Cu^+$·CO configurations as shown in table 2.

### *MO diagram of the $Cu^+$·(CO) complex*

As shown in figure 2, the bonding properties are investigated by examining the MO diagram of CO in the $Cu^+$·(CO) complex at three different configurations: global, local, and transition state structures using NBO population analysis of each energy level of the MO diagram. These calculations are performed on the basis of the B3P86/LANL2DZ/6-311+G (df) method. For the $Cu^+$·CO complex in its global minimum, the interaction of CO with $Cu^+$ ion is formed by donation of the carbon lone pair {sp hybridization} to the 4s orbital of the metal ion to form a $\sigma$-bond. Therefore, the delocalization of carbon lone pair into the 4s orbital is responsible for decreasing the positive charge on the copper ion. For the local minimum and T-shaped structures, the MO diagram indicates that the interaction between them is of purely electrostatic nature where the electrons of the CO valence shell are reorganized. Consequently, a small amount of electronic population migrated toward the antibonding orbitals and tending to lengthen the CO bond as observed in table 1.

### *The $Cu^+$·$(CO)_2$ and $Cu^+$·$(CO)_3$ complexes*

The optimized geometries for the $Cu^+$·$(CO)_2$, in its singlet state ($^1A_1$), and $Cu^+$·$(CO)_3$, in its singlet state ($^1A_1$), complexes are displayed in figures 3 and 4, respectively. The IRC test

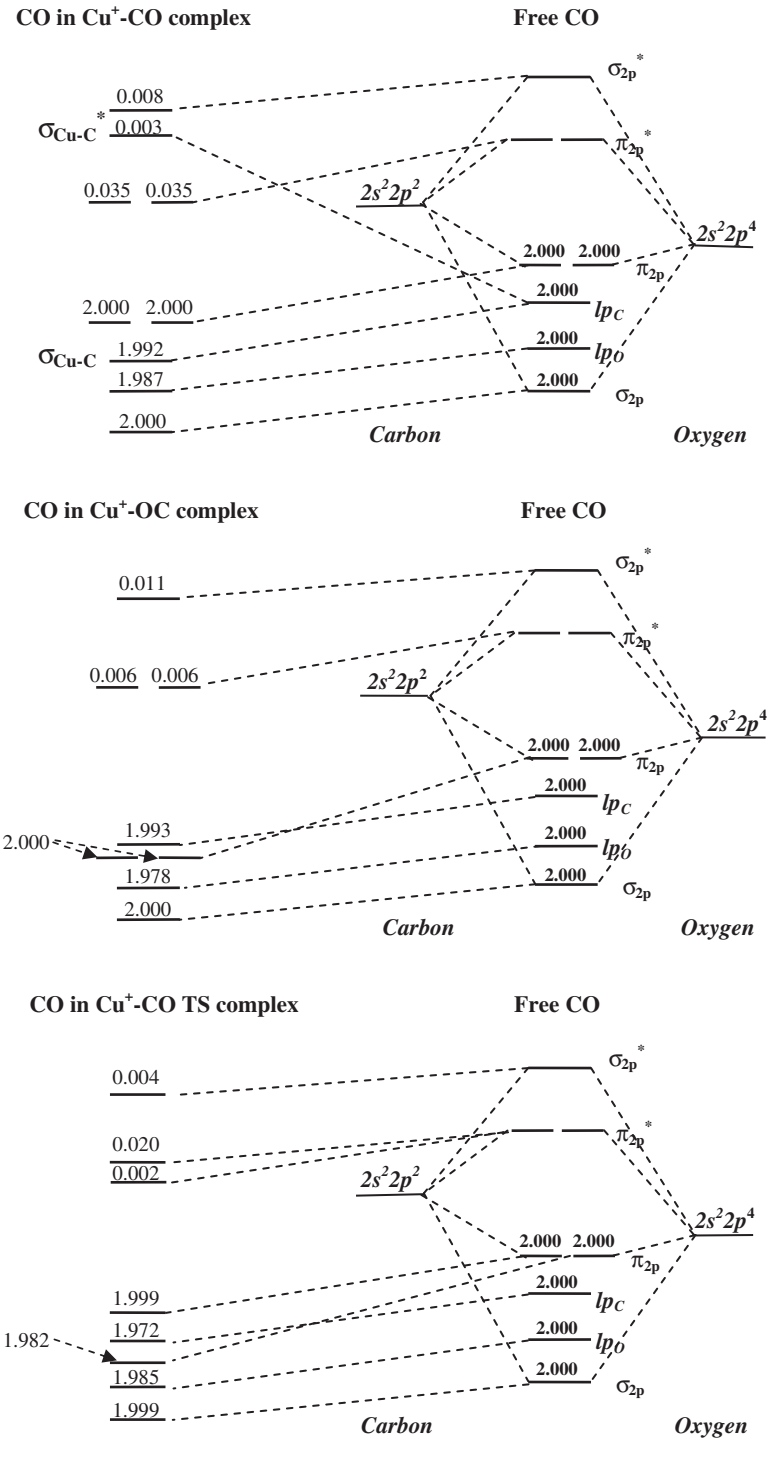


Figure 2. NBO analysis results of the MO diagram of CO at different structures of the $Cu^{+}$·(CO) complex calculated on the basis of the B3P86/LANL2DZ/6-311+G(df) method.
Note: The numbers above each CO level represent their populations.

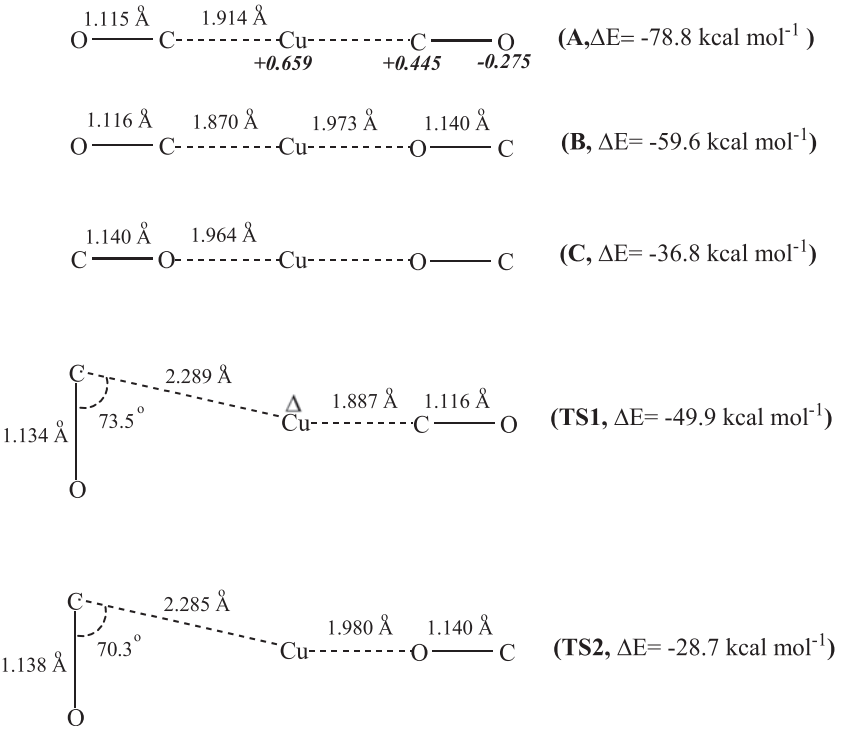


Figure 3. Optimized structures for the minima and transition states of the $Cu^{+}\cdot(CO)_2$ complex obtained on the basis of the B3P86/LANL2TZ+/6-311+G(df) method. The solid italic numbers represent the NBO analysis of the atomic charges of the global minimum structure **A**.

for $Cu^{+}\cdot(CO)_2$ shows three minima of linear configuration and two transition states of T-shaped structure as shown in figure 5. The global minimum, structure **A**, is obtained when the $Cu^{+}$ ion is bonded with each carbon site of the two carbonyl ligands, whereas the other two local minima exhibit the same configuration. The first one, structure **B**, is formed when the two CO molecules approach to the $Cu^{+}$ ion with C and O, respectively. The second approach is both CO molecules approach to the $Cu^{+}$ ion with only O sites (structure **C**). These structures are presented in figure 3. For the $Cu^{+}\cdot(CO)_3$ complex, the potential energy surface of this complex is explored using the IRC test (see figure 6). Our findings show the existence of four minima and three transition state structures. The global minimum is formed when $Cu^{+}$ is bonded with each C site of the three CO molecules in a trigonal planar structure (see figure 4, structure **D**). For the other three local minima, the $Cu^{+}$ is bonded with C and O sites of different CO molecules in a trigonal planar geometry {**E**, **F,** and **G** structures, see figure 4}. The geometry optimization on the singlet potential surface leads to a T-shaped structure for the three transition states as presented in figure 4.

To understand the bonding of the $Cu^{+}\cdot CO$ system and determine the preferable coordination state of the $Cu^{+}$ with CO, the interaction between $Cu^{+}$ ion and four CO molecules is taken into account. The tetra-ligated complex, in its singlet state ($^1A_1$), is only examined in two cases: $Cu^{+}\cdot(CO)_4$ "structure **H**" and $Cu^{+}\cdot(OC)_4$ "structure **I**" complexes. Our DFT calculations show that both complexes adopt relatively the same tetrahedral geometry as presented in figure 7. The Cu–C distances in structure **H** (1.973 Å) are shorter than the

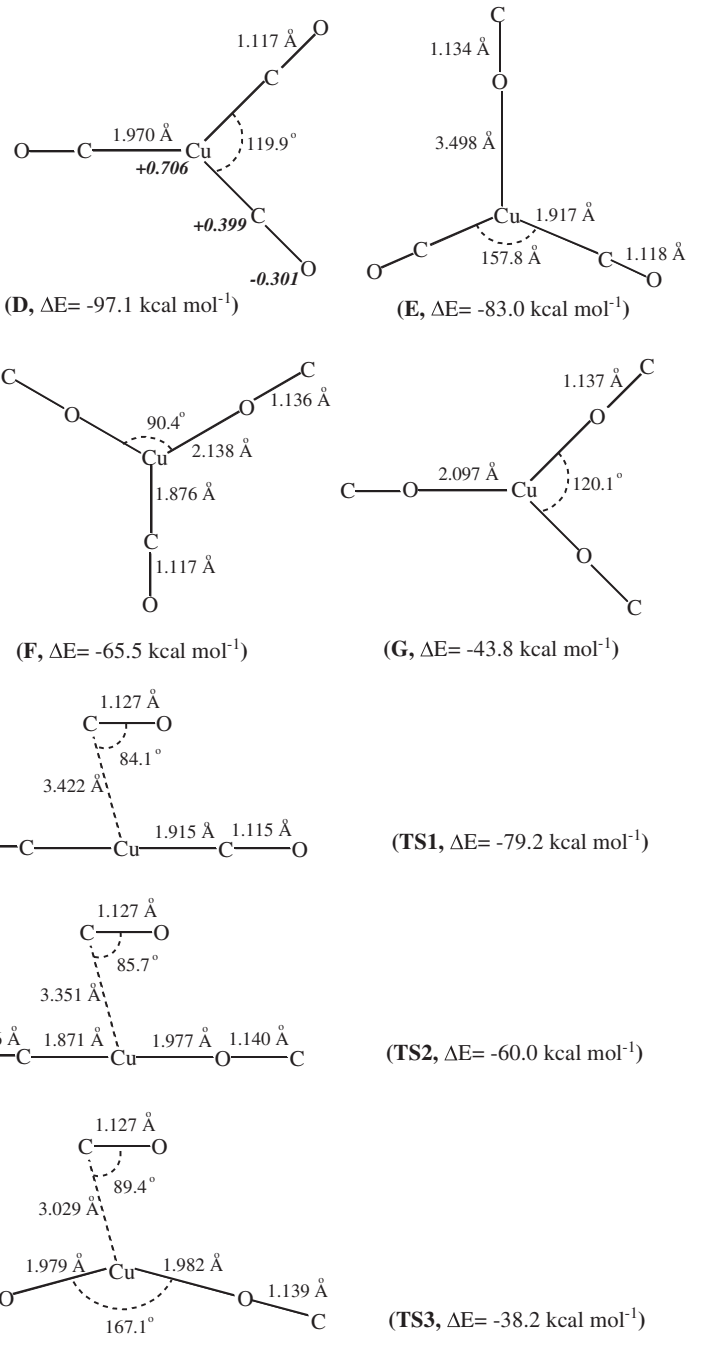


Figure 4. Optimized structures for the minima and transition states of the $Cu^{+}\cdot(CO)_3$ complex obtained on the basis of the B3P86/LANL2TZ+/6-311+G(df) method. The solid italic numbers represent the NBO analysis of the atomic charges of the global minimum structure **D**.

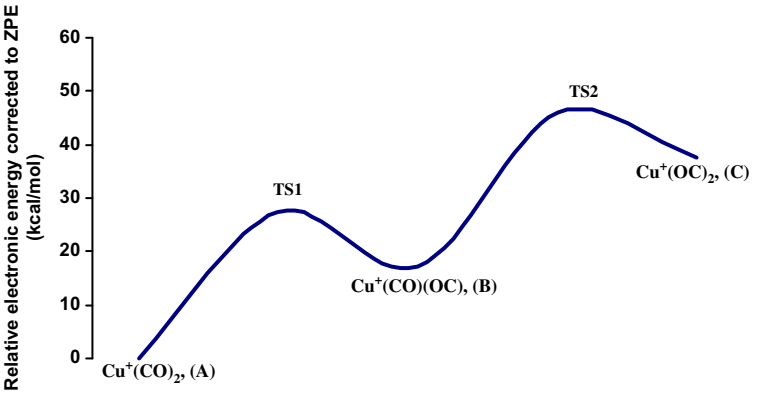


Figure 5. The IRC diagram of the $Cu^{+}\cdot(CO)_2$ complex generated at the B3LYP/LANL2DZ/6-311+G(df) level.

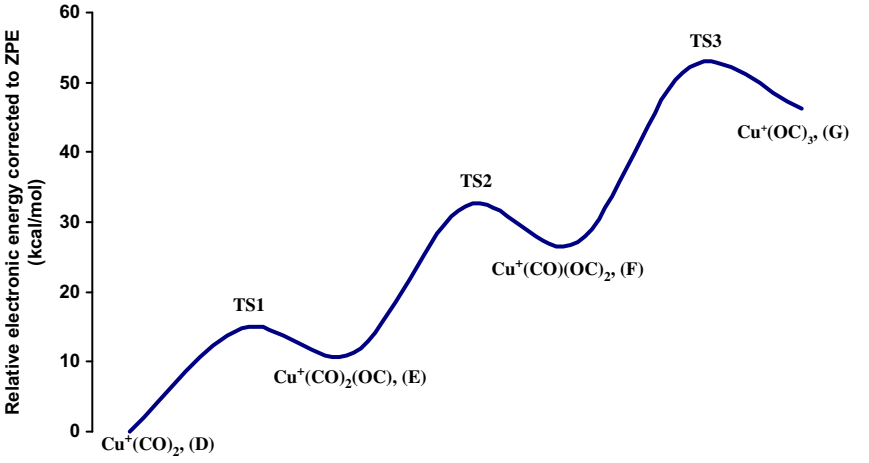


Figure 6. The IRC diagram of the $Cu^{+}\cdot(CO)_3$ complex generated at the B3LYP/LANL2DZ/6-311+G(df) level of theory.

Cu–O distances (2.125 Å) in structure **I**. Therefore, it is expected that the BE of $Cu^{+}$ ion with C sites is stronger than that with O sites for the tetra-ligated complex. Table 3 shows the configurations of CO interacting with $Cu^{+}$ via carbon have larger $\sigma$-donation, ($l$p $\rightarrow$ 4s), than those of *using* oxygen. Similar findings are also obtained for weaker $\pi$-back donation that lies in the range of 0.04–0.08 as shown in figure 3. For the C-coordination complexes, the Cu–C distance in $Cu^{+}\cdot(CO)_2$, **A**, is the shortest among these complexes. In addition, the Cu–C distances increase linearly going from di- to tetra-ligated complexes, {$Cu^{+}\cdot(CO)_2$, **A** $\rightarrow$ $Cu^{+}\cdot(CO)_3$, **D** $\rightarrow$ $Cu^{+}\cdot(CO)_4$, **H**}, as shown in figures 3, 4 and 7. The Cu–C bond strength is also reflected by the calculated $\sigma$-donation, in which the di-ligated complex exhibits the largest $\sigma$-donation (table 3). The variation of the geometry from linear for the $Cu^{+}\cdot(CO)_2$ complex to tetrahedral for the $Cu^{+}\cdot(CO)_4$ complex leads to an increase in the Cu–C distance by ~0.1 Å and hence reducing the $\sigma$-donation as predicted. Similar observations are also obtained for the O-coordination complexes, in which the di-ligated complex, $Cu^{+}\cdot(OC)_2$, **C**, has the shortest Cu–O distances and largest $\sigma$-donation among these four ion

Table 3. NBO analysis of natural charge, 3d, and 4s populations of $Cu^+$ in $Cu^+\cdot(CO)_n$ ($n$ = 2–4) complexes at different orientations on the basis of B3P86/LANL2DZ/6-311+G(df) method.

| Configuration | Symmetry | $q_{Cu}$ | 3d | 4s | $\sigma$-donation (C/$O_{lp} \rightarrow$ 4s) | $\pi$-back donation (3d $\rightarrow \pi^*_{2p}$) |
|---|---|---|---|---|---|---|
| $Cu^+$ | – | +1.000 | 10.000 | 0.000 | – | – |
| $Cu^+\cdot(CO)_2$ (A, global) | $D_{\infty\ h}$ | +0.690 | 9.799 | 0.512 | 0.311 | 0.078 |
| $Cu^+\cdot(CO)(OC)$ (B, local) | $C_{\infty\ v}$ | +0.830 | 9.820 | 0.349 | 0.199 | 0.062 |
| $Cu^+\cdot(OC)_2$ (C, local) | $D_{\infty\ h}$ | +0.937 | 9.898 | 0.163 | 0.148 | 0.038 |
| $Cu^+\cdot(CO)_3$ (D, global) | $D_{3h}$ | +0.738 | 9.783 | 0.479 | 0.269 | 0.072 |
| $Cu^+\cdot(CO)_2(OC)$ (E, local) | $C_{2v}$ | +0.729 | 9.801 | 0.467 | 0.254 | 0.070 |
| $Cu^+\cdot(OC)_2(CO)$ (F, local) | $C_{2v}$ | +0.851 | 9.850 | 0.298 | 0.142 | 0.084 |
| $Cu^+\cdot(OC)_3$ (G, local) | $D_{3h}$ | +0.975 | 9.914 | 0.109 | 0.114 | 0.063 |
| $Cu^+\cdot(CO)_4$ (H, global) | *Td* | +0.744 | 9.755 | 0.492 | 0.247 | 0.081 |
| $Cu^+\cdot(OC)_4$ (I, local) | *Td* | +0.958 | 9.936 | 0.099 | 0.095 | 0.060 |

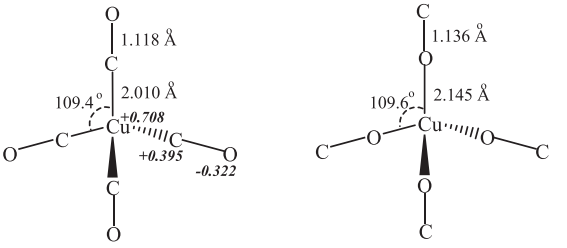


**(H,** ΔE= -112.1 kcal $mol^{-1}$**)** **(I,** ΔE= -50.1 kcal $mol^{-1}$**)**

Figure 7. Optimized structures for the $Cu^+\cdot(CO)_4$ and $Cu^+\cdot(OC)_4$ complexes obtained on the basis of the B3P86/LANL2TZ+/6-311+G(df) method. The solid italic numbers represent the NBO analysis of the atomic charges of structure **H**.

Table 4. BE, thermodynamic quantities, $\Delta H^\circ_{298}$, $\Delta G^\circ_{298}$, and BSSE for $Cu^+\cdot CO$ at the level of various DFT methods. The units are in kcal $mol^{-1}$.

| Geometry | Method | Basis set | BE | $\Delta H^\circ_{298}$ | $\Delta G^\circ_{298}$ | BSSE |
|---|---|---|---|---|---|---|
| Linear $Cu^+\cdot CO$ | B3LYP | LANL2TZ+/6-311+G(df) | 35.2 | −35.9 | −28.3 | 1.75 |
| | B3PW91 | LANL2TZ+/6-311+G(df) | 35.2 | −36.0 | −28.3 | 1.82 |
| | B3P86 | LANL2TZ+/6-311+G(df) | 37.0 | −37.8 | −30.1 | 1.84 |
| | Exp.[a] | – | 35.5 ± 1.6 | – | – | – |
| | MCPF[b] | ECP/primitive Gaussian sets (d,p) | 33.4 | – | – | – |
| | BLYP[c] | TZP | 30.4 | – | – | – |
| | B3LYP[d] | cc-PTVZ/6-31++G** | 37.0 | – | – | – |
| Linear $Cu^+\cdot OC$ | B3LYP | LANL2TZ+/6-311+G(df) | 16.0 | −16.4 | −9.6 | 1.21 |
| | B3PW91 | LANL2TZ+/6-311+G(df) | 14.5 | −14.9 | −8.1 | 1.27 |
| | B3P86 | LANL2TZ+/6-311+G(df) | 16.1 | −16.5 | −9.6 | 1.30 |
| T-shaped TS | B3LYP | LANL2TZ+/6-311+G(df) | 8.1 | – | – | 0.84 |
| | B3PW91 | LANL2TZ+/6-311+G(d) | 7.6 | – | – | 0.78 |
| | B3P86 | LANL2TZ+/6-311+G(d) | 8.9 | – | – | 0.86 |

[a]Taken from Ref. [8].
[b]Taken from Ref. [36].
[c]Taken from Ref. [6].
[d]Taken from Ref. [11].

complexes as presented in figures 3, 4 and 7. Our calculations show that $\sigma$-donation is important for the $Cu^+ \cdot CO$ interaction, whereas the $\pi$-back donation has little influence on these complexes. These findings are consistent with previously MO CI calculations of the $Cu^+ \cdot CO$ complex [7].

### *BEs of the $Cu^+ \cdot CO$ complex*

The BE of $Cu^+ \cdot CO$ complex, at different orientations, is calculated using the basis of different levels of hybrid DFT/LANL2TZ+/6-311+G(df) methods as shown in table 4. For linear $Cu^+ \cdot CO$ global minimum, we quote a best value of 35.2 kcal $mol^{-1}$ that is calculated at the B3LYP level of theory. This value agrees well with the previously reported values by Bauschlicher *et al*. obtaining a best value of 33.4 kcal $mol^{-1}$ [36], Hass *et al*. obtaining a value of 39.3 kcal $mol^{-1}$ [9] and Bell *et al*. calculating a value of 37.0 kcal $mol^{-1}$ [11]. Our best value is also in agreement with the experimental BE of 35.5 ± 1.6 kcal $mol^{-1}$ [8]. For

Table 5. BE, thermodynamic quantities, $\Delta H°$, $\Delta G°$, and BSSE for the $Cu^+ \cdot (CO)_2$ and $Cu^+ \cdot (CO)_3$ complexes at the level of various DFT methods. The units are in kcal $mol^{-1}$.

| Structure | Method | Basis set | BE | $\Delta H°$ | $\Delta G°$ | BSSE |
|---|---|---|---|---|---|---|
| $Cu^+$–$(CO)_2$ (A) | B3LYP | LANL2TZ+/6-311+G(df) | 71.6 | −72.9 | −55.1 | 3.16 |
| | B3PW91 | LANL2TZ+/6-311+G(df) | 71.9 | −73.2 | −53.8 | 3.33 |
| | B3P86 | LANL2TZ+/6-311+G(df) | 75.5 | −76.8 | −57.3 | 3.34 |
| | MCPF[a] | ECP/primitive Gaussian sets (d,p) | 68.9 | – | – | – |
| $Cu^+$–CO)(OC) (B) | B3LYP | LANL2TZ+/6-311+G(df) | 54.1 | −55.1 | −37.9 | 2.96 |
| | B3PW91 | LANL2TZ+/6-311+G(df) | 55.5 | −56.5 | −37.7 | 2.50 |
| | B3P86 | LANL2TZ+/6-311+G(df) | 59.0 | −60.0 | −41.1 | 2.56 |
| $Cu^+$–$(OC)_2$ (C) | B3LYP | LANL2TZ+/6-311+G(df) | 33.3 | −34.1 | −17.6 | 2.91 |
| | B3PW91 | LANL2TZ+/6-311+G(df) | 32.9 | −33.6 | −16.3 | 2.43 |
| | B3P86 | LANL2TZ+/6-311+G(df) | 36.3 | −37.0 | −19.6 | 2.46 |
| T-shaped TS1 | B3LYP | LANL2TZ+/6-311+G(df) | 44.1 | – | – | 2.56 |
| | B3PW91 | LANL2TZ+/6-311+G(df) | 46.3 | – | – | 2.20 |
| | B3P86 | LANL2TZ+/6-311+G(df) | 49.5 | – | – | 2.25 |
| T-shaped TS2 | B3LYP | LANL2TZ+/6-311+G(df) | 25.2 | – | – | 2.07 |
| | B3PW91 | LANL2TZ+/6-311+G(df) | 25.0 | – | – | 2.44 |
| | B3P86 | LANL2TZ+/6-311+G(df) | 28.4 | – | – | 2.30 |
| $Cu^+$–$(CO)_3$ (D) | B3LYP | LANL2TZ+/6-311+G(df) | 89.7 | −91.1 | −66.1 | 2.01 |
| | B3PW91 | LANL2TZ+/6-311+G(df) | 89.8 | −91.3 | −66.1 | 2.29 |
| | B3P86 | LANL2TZ+/6-311+G(df) | 95.0 | −96.5 | −71.3 | 2.13 |
| $Cu^+$–$(CO)_2 \cdot (OC)$ (E) | B3LYP | LANL2TZ+/6-311+G(df) | 77.9 | −78.8 | −55.7 | 1.26 |
| | B3PW91 | LANL2TZ+/6-311+G(df) | 77.2 | −78.1 | −54.9 | 1.29 |
| | B3P86 | LANL2TZ+/6-311+G(df) | 81.6 | −82.6 | −59.2 | 1.40 |
| $Cu^+$–$(OC)_2 \cdot (CO)$ (F) | B3LYP | LANL2TZ+/6-311+G(df) | 61.6 | −62.3 | −39.6 | 0.93 |
| | B3PW91 | LANL2TZ+/6-311+G(df) | 59.6 | −60.3 | −37.8 | 1.32 |
| | B3P86 | LANL2TZ+/6-311+G(df) | 64.5 | −65.2 | −42.8 | 1.00 |
| $Cu^+$–$(OC)_3$ (G) | B3LYP | LANL2TZ+/6-311+G(df) | 41.8 | −42.1 | −21.5 | 0.94 |
| | B3PW91 | LANL2TZ+/6-311+G(df) | 38.5 | −38.7 | −18.0 | 0.88 |
| | B3P86 | LANL2TZ+/6-311+G(df) | 42.8 | −43.0 | −22.2 | 0.98 |
| T-shaped TS1 | B3LYP | LANL2TZ+/6-311+G(df) | 73.5 | – | – | 4.50 |
| | B3PW91 | LANL2TZ+/6-311+G(df) | 71.1 | – | – | 4.08 |
| | B3P86 | LANL2TZ+/6-311+G(df) | 74.9 | – | – | 4.22 |
| T-shaped TS2 | B3LYP | LANL2TZ+/6-311+G(df) | 55.8 | – | – | 4.46 |
| | B3PW91 | LANL2TZ+/6-311+G(df) | 52.7 | – | – | 4.16 |
| | B3P86 | LANL2TZ+/6-311+G(df) | 55.7 | – | – | 4.29 |
| T-Shaped TS3 | B3LYP | LANL2TZ+/6-311+G(df) | 34.9 | – | – | 4.35 |
| | B3PW91 | LANL2TZ+/6-311+G(df) | 30.7 | – | – | 4.11 |
| | B3P86 | LANL2TZ+/6-311+G(df) | 33.9 | – | – | 4.27 |

[a]Taken from Ref. [36].

Table 6. Sequential BDE and BSSE for $Cu^{+}\cdot(CO)_n$ ($n$ = 1-4) calculated at various levels of DFT. The units are in kcal $mol^{-1}$.

| Structure | Method | Basis set | BDE | BSSE |
|---|---|---|---|---|
| *The $Cu^{+}\cdot CO$ complex* | | | | |
| Linear $Cu^{+}\cdot CO$ | B3LYP | LANL2TZ+/6-311+G(df) | 35.2 | 1.75 |
| | B3PW91 | LANL2TZ+/6-311+G(df) | 35.2 | 1.82 |
| | B3P86 | LANL2TZ+/6-311+G(df) | 37.0 | 1.84 |
| | MCPF[a] | ECP/primitive Gaussian sets (d,p) | 33.4 | – |
| | Exp.[b] | – | 35.5 ± 1.6 | – |
| | B3LYP[c] | cc-PTVZ/6-31++G** | 37.0 | – |
| | B3LYP[d] | cc-pVTZ/TZV2P | 36.0 | – |
| | CCSD(T)[e] | aug-pseudopot./6-31G(d) | 30.9 | |
| Linear $Cu^{+}\cdot OC$ | B3LYP | LANL2TZ+/6-311+G(df) | 16.0 | 1.21 |
| | B3PW91 | LANL2TZ+/6-311+G(df) | 14.5 | 1.27 |
| | B3P86 | LANL2TZ+/6-311+G(df) | 16.1 | 1.30 |
| *The $Cu^{+}\cdot(CO)_2$ complex* | | | | |
| $(CO)\cdot Cu^{+}$–CO (A) | B3LYP | LANL2TZ+/6-311+G(df) | 35.6 | 2.44 |
| | B3PW91 | LANL2TZ+/6-311+G(df) | 35.8 | 2.62 |
| | B3P86 | LANL2TZ+/6-311+G(df) | 38.3 | 2.61 |
| | MCPF[a] | ECP/primitive Gaussian sets (d,p) | 35.5 | – |
| | Exp.[b] | – | 41.1 ± 0.7 | – |
| | B3LYP[c] | cc-PTVZ/6-31++G** | 38.0 | – |
| | B3LYP[d] | cc-pVTZ/TZV2P | 35.3 | – |
| | CCSD(T)[e] | aug-pseudopot./6-31G(d) | 34.3 | |
| $(OC)\cdot Cu^{+}$–OC (C) | B3LYP | LANL2TZ+/6-311+G(df) | 17.4 | 1.66 |
| | B3PW91 | LANL2TZ+/6-311+G(df) | 15.9 | 1.79 |
| | B3P86 | LANL2TZ+/6-311+G(df) | 17.6 | 1.82 |
| *The $Cu^{+}\cdot(CO)_3$ complex* | | | | |
| $(CO)_2\cdot Cu^{+}$–CO (D) | B3LYP | LANL2TZ+/6-311+G(df) | 13.7 | 1.96 |
| | B3PW91 | LANL2TZ+/6-311+G(df) | 14.8 | 2.13 |
| | B3P86 | LANL2TZ+/6-311+G(df) | 16.6 | 2.13 |
| | Exp.[b] | – | 17.9 ± 1.0 | – |
| | B3LYP[c] | cc-PTVZ/6-31++G** | 18.0 | – |
| | B3LYP[d] | cc-pVTZ/TZV2P | 16.1 | – |
| | CCSD(T)[e] | aug-pseudopot./6-31G(d) | 17.3 | – |
| $(OC)_2\cdot Cu^{+}$–OC (G) | B3LYP | LANL2TZ+/6-311+G(df) | 5.3 | 1.29 |
| | B3PW91 | LANL2TZ+/6-311+G(df) | 4.6 | 1.40 |
| | B3P86 | LANL2TZ+/6-311+G(df) | 5.5 | 1.46 |
| *The $Cu^{+}\cdot(CO)_4$ complex* | | | | |
| $(CO)_3\cdot Cu^{+}$–CO (H) | B3LYP | LANL2TZ+/6-311+G(df) | 10.1 | 2.08 |
| | B3PW91 | LANL2TZ+/6-311+G(df) | 11.3 | 2.31 |
| | B3P86 | LANL2TZ+/6-311+G(df) | 12.7 | 2.29 |
| | Exp.[b] | – | 12.7 ± 0.7 | – |
| | B3LYP[c] | cc-PTVZ/6-31++G** | 13.0 | – |
| | B3LYP[d] | cc-pVTZ/TZV2P | 13.1 | – |
| | CCSD(T)[e] | aug-pseudopot./6-31G(d) | 14.7 | – |
| $(OC)_3\cdot Cu^{+}$–OC (I) | B3LYP | LANL2TZ+/6-311+G(df) | 4.7 | 1.34 |
| | B3PW91 | LANL2TZ+/6-311+G(df) | 4.1 | 1.45 |
| | B3P86 | LANL2TZ+/6-311+G(df) | 4.9 | 1.43 |

[a]Taken from Ref. [36].
[b]Taken from Ref.[8].
[c]Taken from Ref. [11].
[d]Taken from Ref. [13].
[e]Taken from Ref. [12].

the linear $Cu^{+}\cdot OC$ local minimum, our calculations show that the complex exhibits less BE than that of the global linear structure by a value of 19.0 kcal $mol^{-1}$. This can be

understood in terms of $\sigma$-donation that is stronger for C coordination to $Cu^+$ than that for O coordination to $Cu^+$ as presented in table 2. The T-shaped structure exhibits the least BE of 8.0 kcal $mol^{-1}$, which is consistent with the IRC test findings as shown in figure 1.

### *BEs of the $Cu^+\cdot(CO)_2$ and $Cu^+\cdot(CO)_3$ complexes*

The BE of the carbonyl copper ion complexes, in which $Cu^+$ ion is bonded with two to three CO ligands has been calculated and listed in table 5. Preliminary calculations indicate a strong tendency for the C site of CO to bind to the $Cu^+$ ion. Obviously, the BE of these complexes at different configurations increases with increasing number of carbon sites bonded to $Cu^+$ ion. The calculated BEs for the $Cu^+\cdot(CO)_2$ global minimum is between 72.5 and 76.0 kcal $mol^{-1}$, depending on the level of the method. In this case, the B3LYP and B3PW91 results agree well with another theoretical value of 69.8 kcal $mol^{-1}$, calculated using the basis of the SCF/MCPF method [36]. For the other two local minima, their BEs are lower, 55.6 and 34.9 kcal $mol^{-1}$ for the $Cu^+\cdot(CO)(OC)$ and $Cu^+\cdot(OC)_2$, respectively. The variation in the BE between these minima reflects the strength of the $\sigma$-donation calculated using the NBO population analysis (table 3).

Similar findings were obtained for the $Cu^+\cdot(CO)_3$ complex. The global minimum is obtained when $Cu^+$ is bonded with all carbon sites of the three CO molecules with a BE of 88.8 kcal $mol^{-1}$ [on the basis of the B3LYP/LANL2TZ/6-311+G(df) method]. For each transition state, its BE is lower than that of the two minima on the PES (table 5 and figure 6).

### *Sequential bond energies of $Cu^+\cdot(CO)_n$ (n: 1–4)*

The BDEs of $Cu^+\cdot(CO)$, $Cu^+\cdot(CO)_2$, $Cu^+\cdot(CO)_3$, and $Cu^+\cdot(CO)_4$ at different configurations are calculated using various DFT methods and the results are listed in table 6. For the C- or O-coordinated complexes, the B3P86 calculations shows that the di-ligated complexes have the largest BDE value which agrees well with the experimental findings [8], whereas the tetra-ligated complexes have the least BDE. Note here that our best value (38.3 kcal $mol^{-1}$, calculated on the basis of the B3P86/LANL2TZ+/6-311+G(df) method) of the BDE for $Cu^+\cdot(CO)_2$ lies below the lower end of the experimental range of the BDE (40.4 kcal $mol^{-1}$), whereas the B3LYP and B3PW91 calculations fail to match the experimental findings, since the mono- and di-ligated complexes have the same BDE values as presented in table 6.

To explain the sequential BDE trend observed experimentally, the NBO analysis of the atomic charge distribution of $Cu^+\cdot(CO)_{1-4}$ for the global minima configurations are

Table 7. The electrostatic contribution, $E_{elec.}$, to the BDEs of the C-coordination $Cu^+\cdot(CO)_n$ ($n$ = 1–4) complexes calculated based on atomic charge distributions of these complexes based on the B3P86/LANL2TZ+/6-311+G(df) method (see figures 3, 4 and 7). The NBO analysis of the atomic charges of $Cu^+\cdot CO$ is ***+0.910*** ***+0.359*** ***-0.270*** Cu---------C——O.

| Structure | $E_{elec.}$ (kcal $mol^{-1}$)* |
|---|---|
| $Cu^+\cdot CO$ | −30.8 |
| $Cu^+\cdot(CO)_2$ | −31.5 |
| $Cu^+\cdot(CO)_3$ | −25.1 |
| $Cu^+\cdot(CO)_4$ | −22.6 |

*Calculated using equation (3).

calculated using the B3P86/LANL2TZ+/6-311+G(df) method and presented in figures 3, 4 and 7. The geometrical parameters with their atomic charges are used to calculate the electrostatic energy contribution to the BDE using equation (2). These results are listed in table 7. Our calculations show that di-ligated C-coordinated complexes have the largest electrostatic energy and the variations in the electrostatic energy match the observed experimental trend, where a slight increase in the electrostatic energy is noticed as going from $n = 1$ to $n = 2$ followed by a decrease in the electrostatic energy as going from $n = 2$ to $n = 4$. The variation in the electrostatic energy is consistent with the changes in the $\sigma$-donation and the Cu–C separations presented in table 3 and figures 3, 4 and 7. Our DFT calculations predict that the electrostatic energy and BDEs follow the same order $Cu^+\cdot(CO) < Cu^+\cdot(CO)_2 > Cu^+\cdot(CO)_3 > Cu^+\cdot(CO)_4$ which agree with the experimental findings [8].

Compared to the reported theoretical calculations of the successive CO dissociation energies [11–13] for the reaction: $Cu^+\cdot(CO)_n \rightarrow Cu^+\cdot(CO)_{n-1} + CO$ ($n = 1$, 2, 3, and 4), our best values of the BDE calculated using the B3P86/LANL2TZ+/6-311+G(df) method agree very well with all theoretical results that used DFT calculations. Our DFT calculations yielded better results and closest to the experimental findings than those of CCSD(T) [11] for the mono- and di-ligated carbonyl copper ion complexes as shown in table 6.

## Conclusion

We have presented a DFT study of the electronic structures and BEs of the $Cu^+\cdot(CO)_n$ complexes, $n = 1$–3 and transition states of their conversions. For the $Cu^+\cdot(CO)$ and $Cu^+\cdot(CO)_2$ complexes, a linear structure is obtained for the global and local minima, whereas a T-shaped structure is adopted for all transition states. For $Cu^+\cdot(CO)_3$, trigonal planar geometry is obtained for both global and local minima. The computed BDEs of the $Cu^+\cdot(CO)_n$ ($n = 1$–4) are in excellent agreement with the reported experimental data as well as theoretical calculation results.

Our calculations show that $Cu^+$ prefers to bind to two CO molecules. Furthermore, the $\sigma$-donation strongly affects the interaction, especially when $Cu^+$ is bonded with C site of CO, whereas the electrostatic interaction is an important factor controlling the strength of bonding between $Cu^+$ ion and C/O atomic site of CO. For C-end/O-end coordination of the $Cu^+\cdot(CO)_n/Cu^+\cdot(OC)_n$ complexes, the second ligand has the highest BDE compared to the others because of the higher efficiency of $\sigma$-donation, shorter Cu–C/O separation and stronger electrostatic interactions.

## Acknowledgement

JND would like to thank the Deanship of the Graduate Studies of the Hashemite University (Jordan) for the financial support.

## References

[1] A. Stern, R. Boubel, D. Turner, D. Fox. *Fundamentals of Air Pollution*, 2nd Edn, Academic Press, Orlando, FL (1984).
[2] K.C. Taylor. *Catal. Rev. - Sci. Eng.*, **35**, 457 (1993).

[3] C. Lamberti, P.G. Turnes, S. Bordiga, G. Berlier, F. D'Acapito, A. Zecchina. *Angew. Chem. Int. Ed.*, **39**, 2138 (2000).
[4] W. Zhang, M. Jia, J. Yu, T. Wu. *Chem. Mater.*, **11**, 920 (1999).
[5] E. Broclawik, J. Datka, B. Gil, W. Piskorz, P. Kozyra. *Top. Catal.*, **11/12**, 335 (2000).
[6] C. Briones-Jurado, E. Agacino-Valdés. *Int. J. Quantum Chem.*, **108**, 1802 (2008).
[7] M. Merchán, I. Nebot-Gil, R. González-Luque, E. Ortí. *J. Chem. Phys.*, **87**, 1690 (1987).
[8] F. Mayer, Y. Chen, P.B. Armentrout. *J. Am. Chem. Soc.*, **117**, 4071 (1995).
[9] W. Schneider, K. Hass, R. Ramprasad, J. Adams. *J. Phys. Chem.*, **100**, 6032 (1996).
[10] P. Treesukol, J. Limtrakul, T. Truong. *J. Phys. Chem. B*, **105**, 2421 (2001).
[11] X. Zheng, Y. Zhang, T. Bell. *J. Phys. Chem. C*, **111**, 13442 (2007).
[12] A. Lupinetti, V. Joans, W. Thiel, S. Strauss, G. Frenking. *Chem. Eur. J.*, **5**, 2573 (1999).
[13] G. Wu, Y. Li, H. Xiang, Y. Xu, Y. Sun, H. Jiao. *J. Mol. Struct. (Theochem)*, **637**, 101 (2003).
[14] M. Frisch, G. Trucks, H. Schlegel, G. Scuseria, M. Robb, J. Cheeseman, J. Montgomery, T. Vreven, K. Kudin, J. Burant, J. Millam, S. Iyengar, J. Tomasi, V. Barone, B. Mennucci, M. Cossi, G. Scalmani, N. Rega, G. Petersson, H. Nakatsuji, M. Hada, M. Ehara, K. Toyota, R. Fukuda, J. Hasegawa, M. Ishida, T. Nakajima, Y. Honda, O. Kitao, H. Nakai, M. Klene, X. Li, J. Knox, H. Hratchian, J. Cross, C. Adamo, J. Jaramillo, R. Gomperts, R. Stratmann, O. Yazyev, A. Austin, R. Cammi, C. Pomelli, J. Ochterski, P. Ayala, K. Morokuma, G. Voth, P. Salvador, J. Dannenberg, V. Zakrzewski, S. Dapprich, A. Daniels, M. Strain, O. Farkas, D. Malick, A. Rabuck, K. Raghavachari, J. Foresman, J. Ortiz, Q. Cui, A. Baboul, S. Clifford, J. Cioslowski, B. Stefanov, G. Liu, A. Liashenko, P. Piskorz, I. Komaromi, R. Martin, D. Fox, T. Keith, M. Al-Laham, C. Peng, A. Nanayakkara, M. Challacombe, P. Gill, B. Johnson, W. Chen, M. Wong, C. Gonzalez, J. Pople. *Gaussian 03, Revision B.05*, Gaussian, Inc., Pittsburgh, PA (2003).
[15] D. Feller. *J. Comput. Chem.*, **17**, 1571 (1996).
[16] K. Schchardt, B. Didier, T. Elsethagen, L. Sun, V. Gurumoorthi, J. Chase, J. Li, T. Windus. *J. Chem. Inf. Model.*, **47**, 1045 (2007).
[17] J. Dawoud, I. Fasfous, A. Majdalawieh. *Z. Naturforsch., B*, **67**, 118 (2012).
[18] J. Ducéré, A. Goursot, D. Berthomieu. *J. Phys. Chem. A*, **109**, 400 (2005).
[19] E. Molenbroek, N. Straathof, S. Dück, Z. Rashid, J. Lenthe, M. Lutz, A. Gandubert, R. Gebbink, L. Cola, S. Bonnet. *Dalton Trans.*, **42**, 2973 (2013).
[20] Z. Wu. *Chem. Phys. Lett.*, **383**, 251 (2004).
[21] H. Grönbeck, W. Andreoni. *Chem. Phys.*, **262**, 1 (2000).
[22] G. Theodoor de Jong, R. Visser, F. Bickelhaupt. *J. Organomet. Chem.*, **691**, 4341 (2006).
[23] M. Bühl, C. Reimann, D. Pantazis, T. Bredow, F. Neese. *J. Chem. Theory Comput.*, **4**, 1449 (2008).
[24] C. Cramer, D. Truhlar. *Phys. Chem. Chem. Phys.*, **11**, 10757 (2009).
[25] C. Gonzalez, H. Schlegel. *J. Chem. Phys.*, **90**, 2154 (1989).
[26] C. Gonzalez, H. Schlegel. *J. Phys. Chem.*, **94**, 5523 (1990).
[27] M. Alomari, J. Dawoud. *J. Mol. Struct. (Theochem)*, **939**, 28 (2010).
[28] F. Budenholzer, E. Gislason, A. Jorgensen. *Chem. Phys.*, **110**, 171 (1986).
[29] S. Ikuta. *Chem. Phys. Lett.*, **109**, 550 (1984).
[30] J. Carpenter, F. Weinhold. *J. Mol. Struct. (Theochem)*, **169**, 41 (1988).
[31] J. Foster, F. Weinhold. *J. Am. Chem. Soc.*, **102**, 7211 (1980).
[32] A. Reed, F. Weinhold, L. Curtiss. *Chem. Rev.*, **88**, 899 (1988).
[33] D. Kaur, S. Khanna. *Comput. Theor. Chem.*, **963**, 71 (2011).
[34] G. Blyholder. *J. Phys. Chem.*, **68**, 2772 (1964).
[35] D. Liu, T. Wyttenbach, M. Bowers. *Int. J. Mass Spectrom.*, **236**, 81 (2004).
[36] L. Barnes, M. Rosi, C. Bauschlicher. *J. Chem. Phys.*, **93**, 609 (1990).
[37] J. Harrison. *J. Phys. Chem. A*, **110**, 10848 (2006).
[38] W. Schneider, K. Hass, R. Ramprasad, J. Adams. *J. Phys. Chem. B*, **102**, 3692 (1998).
[39] W. Schneider, K. Hass, R. Ramprasad, J. Adams. *J. Phys. Chem. B*, **101**, 1940 (1997).